THE JOURNAL OF PHYSICAL CHEMISTRY B

Article

Evaluation of a New Biosensor Based on In-Situ Synthesized PPy-Ag-PVP Nanohybrid for Selective Detection of Dopamine

Balakumar Vellaichamy, Prakash Periakaruppan, and Tharmaraj Paulmony

J. Phys. Chem. B, **Just Accepted Manuscript** • DOI: 10.1021/acs.jpcb.6b11225 • Publication Date (Web): 12 Jan 2017

Evaluation of a New Biosensor Based on *In-Situ* Synthesized PPy-Ag-PVP Nanohybrid for Selective Detection of Dopamine

Balakumar Vellaichamy, Prakash Periakaruppan* and Tharmaraj Paulmony

Department of Chemistry, Thiagarajar College, Madurai – 625 009, Tamil Nadu, India.

ABSTRACT

In the present work, *in-situ* synthesis of polypyrrole-silver-polyvinylpyrrolidone (PPy-Ag-PVP) nonohybrid using $AgNO_3$ as an oxidant and polyvinyl pyrrolidone (PVP) as a stabilizer and surfactant is demonstrated. The obtained ternary PPy-Ag-PVP nanohybrid was characterized by UV-vis, FT-IR, XRD, Raman, TGA, SEM and HR-TEM analysis. Further the synthesized PPy-Ag-PVP has been investigated for its selective and sensitive sensing of dopamine (DA). The PPy-Ag-PVP modified glassy carbon electrode shows a reversible electrochemical behavior with superior response for DA. The limit of detection and limit of quantification are found to be 0.0126 and 0.042 μM (S/N = 3 & 10) respectively with remarkable sensitivity (7.26 μA mM^{-1} cm^{-2}). The practical application of the present modified electrode has been validated by determining the concentration of DA in human urine samples of different age group.

Corresponding Author

*E-mail: kmpprakash@gmail.com *Tel: +91 9842993931; Fax: +91 4522312375

1. INTRODUCTION

Dopamine (DA), (also called as 3,4-dihydroxy phenyl ethylamine) is a biological, pharmacological and physiological important neurotransmitter of catecholamine compound which plays a vital role in the function of human metabolism and also human brain for message transfer in the mammalian central nervous, renal and hormonal system.[1, 2] Even a very low concentration (0.01-1μM) of DA in brain tissue is associated with a variety of diseases such as epilepsy, senile dementia, hyperactivity disorders, Parkinson's disease, Alzheimer's disease, schizophrenia, Huntington's disease and even HIV infection.[3–8] Thus, it is necessary to establish a tool for selective and sensitive detection of DA in vivo/vitro in clinical, biomedical and analytical investigations. Several analytical techniques have been developed for the determination of DA in environmental and biological samples.[9-13] However most of these protocols are high-cost, time-consuming, and even relying on special equipment. On the other hand, electrochemical methods have received much interest, because they are more selective, highly sensitive, less time consuming and require simple operation and real time sensing in vivo [14,15] also is possible. In recent years, several surface modification materials such as conducting polymers, metal nanoparticles, self-assembled monolayers, graphene, carbon nanotubes, metal oxide nano particles and composite materials have been intensively developed to increase the performance of electrochemical DA sensors. But the problem associated with the detection efficiency is that DA is oxidized at almost the same potential of ascorbic acid (AA). [16-21] Therefore it is still essential to synthesize new avenue star materials for the selective and sensitive sensing of DA, a crucial target of researchers.

The discovery of conducting polymers has given rise to interesting optical, electronic, and electrical properties that are required by various applications. [22] Among the conducting polymers, polypyrrole (PPy) is the most extensively studied substance owing to its high conductivity, stability, good dispersibility and ease of synthesis. [23] Despite these desirable properties, PPy is a solid insoluble in organic solvents and infusible at processing temperatures, which restrict its processing and potential

uses. [24] Also noble metal nanoparticles (MNPs) have emerged as promising materials in recent years and show inspiring potential in sensing because of their unusual physical and chemical properties. Among them, silver nanoparticles (AgNPs) display excellent electrocatalytic ability towards the redox reaction of DA because of its high surface area, effective mass transport and high catalytic activity. [25-30] However homogeneous silver nanoparticles are undesirable for biological and pharmaceutical applications because of their number of drawbacks, such as easy aggregation or precipitation, less electron transfer properties, and less electrocatalytic stability and recycling.

To tackle these problems, synthesis of PPy composites with different nanomaterials is a common preferred way. But again the main drawback associated with binary PPy-nanomaterials is poor stability and selectivity during sensing process. Hence it is imperative to design and develop a nanocomposite with high surface area, long-term stability, high electrocatalytic activity and reusability, which should be able to promote the kinetics of electron transfer reactions. These features are able to be achieved only by ternary nanocomposite materials such as the one proposed in this article. The main objective of this paper is to report, for the first time, an *in-situ* polymerization of pyrrole using $AgNO_3$ as an oxidant and PVP as a stabilizer and surfactant to form PPy and AgNPs simultaneously. Further the synthesized PPy-Ag-PVP has been investigated for its selective and sensitive sensing of dopamine (DA). The practical application of the present modified electrode has been validated by determining the concentration of DA in human urine samples of different age group.

2. EXPERIMENTAL SECTION

2.1. Chemicals

$AgNO_3$, pyrrole, PVP, DA, AA, uric acid (UA), folic acid (FA), glucose, fructose and sucrose were purchased from Sigma-Aldrich and used as received. Phosphate buffer solutions (PBS) of different pH were prepared using 0.1 M solutions of NaH_2PO_4 and Na_2HPO_4 and adjusting them with

orthophosphoric acid for acidic pH and NaOH for basic pH. All other chemicals were of analytical grade and were used as received without further purification. Double distilled water was used for preparing all the solutions.

2.2. Synthesis of PPy-Ag-PVP

PPy-Ag-PVP has been synthesized via *in-situ* chemical oxidative polymerization method using $AgNO_3$ as an oxidant cum dopant without addition of any other oxidant and reductant. The formation of PPy and Ag nanoparticles are taking place simultaneously. In a typical experiment, 0.1 mg of PVP was dissolved in water. 0.5 ml of pyrrole was added into the above solution and stirred for 30 min. Then the oxidizing agent, here 250 ml (1 mM) of $AgNO_3$, was added drop wise to the reaction system. Polymerization of pyrrole and the formation of silver nanoparticles take place simultaneously in the presence of PVP as a stabilizer and the color of the solution changes from pale yellow to black. The reaction was allowed in dark room for seven days. Finally, the black precipitate (PPy-Ag-PVP) was filtered and washed with a large amount of double distilled water to remove any other unreacted products and dried in an air oven at 60º C for 12 h. The composite is designated as PPy-Ag-PVP (1). Similar procedure was adopted to synthesize PPy-Ag-PVP (2) and (3) by changing the amount of PVP (0.2 and 0.3 mg).

2.3. Preparation of PPy-Ag-PVP modified GCE

The PPy-Ag-PVP modified GCE was prepared firstly by dispersing PPy-Ag-PVP in double distilled water by ultrasonication for 15 min. Then a 5 µL of PPy-Ag-PVP (2) solution was drop casted on the surface of GCE and dried in an air oven. Finally, the modified GCE was used for the detection of DA.

2.4. Instrumentation

UV–vis spectra measurements were obtained with a Jasco (V-560) spectrometer. FT-IR spectrum of each sample was obtained with a model 460 Plus (JASCO) FT-IR spectrometer. The samples were examined by X-ray diffraction (XRD) performed on a JEOL JDX 8030 X- ray diffractometer with Cu Kα radiation (λ = 1.5418^{o} A). Raman spectra were recorded on a Bruker senterra dispersive Raman microscope with laser excitation wavelength of 532 nm. TGA of samples was carried out with a (TGA-50, SHIMADZU) thermogravimetric analyzer at a heating rate of 10º C min^{-1} up to 800º C in nitrogen atmosphere. The morphology of all samples was examined using SEM and HR-TEM. SEM measurements were carried at VEGA3 TESCAN, USA. HR-TEM experiments were performed using a FEI TECNAI T20 G2 instrument and the sample was prepared by casting on a copper grid. The electrochemical measurements were carried out with CHI electrochemical workstation (Model 660E, Austin, TX-USA). Electrochemical measurements were performed in a conventional two-compartment three-electrode cell with GCE as a working electrode, platinum wire as a counter electrode and KCl-saturated Ag/AgCl as a reference electrode. All the electrochemical experiments were carried out under nitrogen atmosphere at room temperature. Scheme 1 shows a schematic representation of *in-situ* synthesis of PPy-Ag-PVP nanohybrid.

3. RESULTS AND DISCUSSION

3.1. UV-Vis Spectroscopy

Surface plasman resonance (SPR) band of MNPs and the oxidation and doping state of the polymeric backbone was confirmed by UV-vis spectroscopy. Figure. 1A shows the UV-vis absorption spectra of PPy-Ag-PVP (1-3) nanohybrid dispersed in water. As can be seen in Figure.1A, PPy-Ag-PVP shows three absorption peaks at 280, 424 and 580 nm. The spectra show a strong transition band appearing at 280 nm, which corresponds to π-π* transition of polymeric backbone coupled with PVP. [31] The band at 620 nm corresponds to the transitions from valence band to the uppermost bipolarons band of PPy. [32]

Furthermore, a sharp and strong absorption band observed at 424 nm is attributed to the SPR of the AgNPs. [33] It is evident from the figure that as the quantity of PVP (0.1 and 0.2 mg) increases, the intensity ratio of PPy-Ag-PVP increases (Figure. 1A (curve a & b)). Further increase of PVP (0.3 mg) decreases (Figure. 1A (curve c)) the peak intensity. Based on the above results, it is observed that 0.2 mg PVP is optimum for the synthesis of PPy-Ag-PVP with high stability.

3.2. FT-IR spectroscopy

FT-IR spectroscopy is a very useful tool for the analysis of interaction between two or more species. Figure. 1B shows the FT-IR spectra of PPy-Ag-PVP (1-3) nanohybrid where several characteristics bands appear. The strong bands appearing at 1545 and 1462 cm^{-1} can be attributed to C–N and C–C asymmetric and symmetric ring-stretching respectively. [34] The peak appearing at 1690 cm^{-1} suggests the existence of chemical bonding between metal ions or metal clusters and PVP. [35] The bands at 2935 and 2850 cm^{-1} of PPy-Ag-PVP are assigned to the symmetric and assymetric vibrations of -CH_2which indicate the alkyl chain of PVP is adsorbed on the PPy-AgNPs. The peaks at 1173 and 895 cm^{-1} correspond to the doping state of PPy and the sharp peak at 1029 cm^{-1} is ascribed to C–H deformation and N–H stretching vibrations. The broad band at 1307 cm^{-1} demonstrates the C–H and C–N in-plane deformation vibration. [36] The peak at 677 cm^{-1} indicates the reduction of the silver ions coupled to the oxidation of the amine components. These results confirm the presence of PVP stabilized AgNPs on the PPy backbone. It is also observed that as the quantity of PVP increases from 0.1 and 0.2 mg the intensity ratio of PPy-Ag-PVP increases (Figure. 1B (curve a & b)). Further increase of PVP (0.3 mg) decreases (Figure. 1B (curve c)) the peak intensity. Therefore again it is confirmed that 0.2 mg of PVP is ideal for the production of stable PPy-Ag-PVP nanohybrid.

3.3. X-Ray Diffraction

XRD can provide valuable information about the crystalline nature and orientation of PPy-Ag-PVP (1-3) nanohybrid. The XRD patterns of PPy-Ag-PVP nanohybrids exhibit characteristic diffraction peak at 2θ=11.9º corresponding to PVP crystalline phase [35] as shown in Figure. 1C (curve a-c). The peak at 26.32^0 is associated with PPy chains with some degree of crystallinity. [23] Further, the diffraction peak at 37.70º, 43.81º, 63.85º and 76.70º correspond to the lattice planes of (1 1 1), (2 0 0), (2 2 0) and (3 1 1) with a face centered cubic (fcc) structure of metallic silver, which is in good agreement with (JCPDS) data [no. 04-0783]. [33] When the quantity of PVP is increased from 0.1 and 0.2 mg the intensity of AgNPs is found to increase as shown Figure.1C (curve a & b). But further increasing the quantity of PVP (0.3 mg) shows in the spectra some unassigned peaks at 33.78º, 56.41º and 67.86º (curve c) which are due to the excess amount of PVP present in the ternary PPy-Ag-PVP nanohybrid. [35] The XRD results also clearly indicate that 0.2 mg of PVP is optimum for the synthesis of stable PPy-Ag-PVP (2) with a high conducting and crystalline nature.

3.4. Raman spectroscopy

Raman spectroscopy is used to further characterize the PVP anchored PPy-AgNPs. The Raman spectra of ternary PPy-Ag-PVP (1-3) nanohybrid are shown in Figure. 1D (curve a-c). The vibrational peaks at 1350 and 1585 cm^{-1} correspond to the PVP stabilized AgNPs. [35] Another three vibrational peaks at 1402, 1088 and 896 cm^{-1} are corresponding to the stretching vibrations of C=N groups, C-H in plane deformation and radical cation (polaron), respectively. [37] The peak at 1600 cm^{-1} is assigned to C=C backbone stretching of PPy. [38] Interestingly, the Raman spectra also clearly shows that the quantity of PVP required for the synthesis of nanohybrid with high stability is 0.2 mg since increase of PVP above 0.2 mg decreases the Raman peak intensity.

3.5 SEM

Scanning electron microscopy (SEM) tests were performed to identify changes in the surface morphology of PPy-Ag-PVP nanohybrid as shown in Figure. 2 (a-c). As seen from Figure. 2 (a), the synthesized PPy-Ag-PVP (1) nanohybrid has a very clean and smooth surface. NPs formation is not complete and the particles are easily aggregated due to lack of PVP. Figure. 2 (b) of PPy-Ag-PVP (2) demonstrates that PVP stabilized spherical AgNPs are well coated over the PPy surface. Figure. 2 (c) of PPy-Ag-PVP (3) shows that excess amount of PVP has covered the PPy-AgNPs. These results suggest that the formation of AgNPs is incomplete in PPy-Ag-PVP (1) and PVP in excess has fleeced on the PPy-Ag-PVP (3).

3.6 HR-TEM

The morphology of PPy-Ag-PVP (1-3) was analyzed by HR-TEM. It can be seen from Figure. 3a of PPy-Ag-PVP (1) that AgNPs are aggregated on to the PPy surface. Figure. 3b of PPy-Ag-PVP (2) illustrates that the spherical shaped AgNPs are coated on the surface of PPy and Figure. 3c of PPy-Ag-PVP (3) clearly demonstrates that the excess of PVP covers AgNPs coated on the PPy surface. These results confirm that the PPy-Ag-PVP (2) preparation is most suitable. This type of varied morphology is attributed to defective structures of nano composite formed in the presence of lower and higher concentration of PVP. On the other hand, the different magnification of PPy-Ag-PVP (2), as shown in Figure. 3d & e, evidently displays the crystalline structure of AgNPs on to the PPy surface. The high-resolution HR-TEM image taken from the nanoparticle (Figure. 3e) reveals clear lattice fringes with an inter planar distance of 0.236 nm corresponding to the (1 1 1) lattice space of metallic Ag. Further selected area electron diffraction (SAED) of PPy-Ag-PVP (2) reveals that the well-defined diffraction circular rings are fully indexed to the (1 1 1), (2 0 0), (2 2 0) and (3 1 1) of the pure face centered cubic (fcc) lattice structure of Ag as shown in Figure 3f. This result is consistent with the XRD

characterizations. Also the TEM analysis results together with the UV-Vis, FT-IR, XRD and Raman spectra confirm that the PPy-Ag-PVP (2) is appropriate material for sensor study vis-à-vis surface area, stability and conductivity.

3.7. TGA

To investigate the thermal stability of the ternary PPy-Ag-PVP (2) nanohybrid, TGA was carried out and the result is shown in Figure. 4. The first weight loss of PPy-Ag-PVP (2) is at a temperature range of 30-175º C, which corresponds to the removal of physically adsorbed water molecules and unreacted dopant ions from the PPy surface [39], which is about 5 % weight loss. A slight weight loss occurs after 175º C due to the decomposition of oligomers present in the PPy chains. The second step of weight loss between 200 and 400º C is due to the loss of PVP and dopant. In the third decomposition step, in the temperature range from 400 to 800º C, the gradual weight loss may be associated with the breakdown of the PPy chains. [40, 41] The total weight loss up to 800º C is assessed to be 33.1 % for the ternary PPy-Ag-PVP (2) nanohybrid. These results suggest that the nanocomposite material synthesized has high thermal stability.

3.8. Electrochemical determination of DA

The electrocatalytic oxidation of DA was studied by the cyclic voltammetry with ternary PPy-Ag-PVP (2) nanohybrid modified electrode at scan rate, 50 mVs^{-1} in the potential range of –0.1 - 1.0 V as shown in Figure. 5A (curve a). It can be seen that dopamine gives a pair of quasi-reversible redox peaks (Figure. 5A (curve b)) at ternary PPy-Ag-PVP (2) nanohybrid modified electrode. The oxidation and reduction peak of DA is observed with the peak potentials at 0.132 V and 0.110 V respectively. These observations with the modified electrode indicate that PPy-Ag-PVP (2) has good electrochemical activity due to the synergistic properties of nanohybrid materials.

3.9. Effect of concentration

To evaluate the reversibility of different concentrations of DA, redox reactions were performed in the potential range from -0.1 to 1.0 V. Figure. 5B shows the CV response of PPy-Ag-PVP (2) with different concentrations of (10- 100 μM) DA containing 0.1 M PBS at scan rate 50 mVs^{-1}. It can be seen from Figure. 5B that as the concentration of DA increases there is no shift in the oxidation peak potential, but a noticeable increase in the peak current is observed, which indicates that the electron transfer kinetic process occurs at PPy-Ag-PVP (2) nanohybrid in the oxidation of DA. As shown in Figure. 5C, the oxidation peak currents have a linear dependence against the concentration of DA from 10-100 μM with the correlation coefficient of 0.9980. These results prove that the PPy-Ag-PVP (2) nanohybrid has good electrocatalytic activity and the reaction mechanism for the electrochemical sensing of DA by a PPy-Ag-PVP (2) is shown in Figure 6.

3.10. Effect of scan rate

Furthermore, to check the reversibility of 50 μM DA redox reactions at the modified electrode, different scan rate studies were performed in the potential range from -0.1- 0.6 V at 0.1 M PBS (pH 7.2) as shown in Figure. 7A. The redox peak currents increase gradually with the increase of scan rate from 50-140 mV s^{-1}. With the increase of scan rate, the oxidation peak potential shifts to the positive direction and the reduction peak potential to the negative direction, indicating a slow electrochemical quasi-reversible behavior of DA at the electrode surface, where the oxidation of DA to o-dopaminoquinone (DAQ) and the reduction of DAQ back to DA, respectively takes place. [42] Figure. 7B shows a plot of logarithm of the peak current for DA versus scan rate, which exhibits a linear relationship in the range of 50–140 mV s^{-1} with the correlation coefficient of 0.9993 and 0.9992. It can be inferred from the slopes that the redox process of DA at PPy-Ag-PVP (2) modified GCE is a diffusion-controlled electrochemical reaction. [43]

3.11. Effect of pH

The electrochemical behaviour of DA at different pH solutions was investigated using CV. As can been seen in Figure.7C, the current response increases from pH 3.0 to 7.2 and it reaches maximum at pH 7.2. A decreasing trend is observed from pH 7.2 to 11. The oxidation and reduction potential of DA shifts negatively and positively with a higher and lower pH value (Figure. 7D), which suggests that the protons are taking part in the electrode reaction process. [44] Hence pH 7.2 is found to be the optimum pH for high selective and sensitive sensing of DA.

3.12. Differential pulse voltammetry

Figure. 8A displays a typical differential pulse voltammetry (DPV) curves corresponding to the electrocatalytic oxidation of DA at PPy-Ag-PVP (2) nanohybrid modified GCE in N_2 saturated PBS. As shown in Figure. 8A, upon increasing the concentration of DA (0.5–22.5 μM) into the 0.1 M PBS, the oxidation peak current observed at 0.2 V exhibits remarkable enhancement linearly (Figure. 8A (curve a-j)) suggesting that PPy-Ag-PVP (2) modified GCE can be applied for the quantitative determination of DA. The oxidation peak current (I_{pa}) of DA has a good linear relationship with DA concentration in the range from 0.5 to 22.5 μM (Figure. 8B) with the correlation coefficient of 0.9943.

3.13. Amperometric i–t curve (Amp)

The fabricated PPy-Ag-PVP (2) nanohybrid was further applied for the determination of DA using amperometric method. Figure. 8C shows the amperometric i–t curve obtained for DA at PPy-Ag-PVP (2) modified GCE in a homogeneously stirred 0.1 M PBS (pH 7.2) by applying a potential of +0.132 V. pThe PPy-Ag-PVP (2) shows the current response for each addition of 100 nM DA in every 50 s interval. The current response increases and the steady state-current response is attained within 5 s. The steady-state current response with respect to concentration of DA shows an excellent linear relation from 100 nM to 900 nM with a correlation coefficient of 0.9778 as shown in Figure. 8D. The limit of

detection and limit of quantification are found to be 0.0128 μM and 0.042 μM for DA (S/N=3 and 10) respectively. The relative standard deviations (RSD) (n = 7) for determination DA is found to be 1.9%. The observed linear range, sensitivity and the detection limit for DA at PPy-Ag-PVP (2) modified GCE have been compared with the other recently reported modified electrodes and are given in Table 1. [25, 45-64] Particularly worth declaring is that our proposed sensor's sensitivity is found to be 7.256 μA mM^{-1} cm^{-2}, which is significantly comparable to other earlier reported DA sensors.

3.14. Interferences, stability and repeatability

Human body always contains a mixture of organic or inorganic small molecules and amino acid, which normally coexist with DA in human blood serum or other samples. Therefore, it is necessary to investigate the 200 nM DA and effect of interferences namely AA, UA, FA, glucose, sucrose and fructose (20 fold excess) on the sensing ability of PPy-Ag-PVP (2) modified GCE as shown in Figure. 9. There is no significant influence of these interferences on the proposed sensor and the current response of the interfering substances can be neglected compared to the response of DA. These results indicate that PPy-Ag-PVP (2) modified GCE can be used as a potential candidate for highly selective and sensitive sensing of DA. The long-term stability of the sensor was investigated over a period of 15 days by storing the composite after sensing in 0.1 M PBS (pH 7.2). The peak current decreases just less than 5 ± 0.05% after the electrode was stored at 4° C for 15 days, which is well evidenced by the electrochemical impedance and FT-IR spectral results as shown in Figure.10 (a & b). To find out the repeatability of the results, two different GCEs were modified with PPy-Ag-PVP (2) and their responses towards 50 μM DA was recorded by 15 repeated cycles. The peak current obtained in the 15 repeated cycles of two independent electrodes show a relative standard deviation of 3.2 ± 0.05%, confirming that the results are repeatable. These results reveal a good anti-interference ability, stability and repeatability of PPy-Ag-PVP (2) towards the sensing of DA sensitively and selectively.

3.15. Real sample analysis

The practical application of the PPy-Ag-PVP (2) modified GCE was tested by measuring the concentration of DA in the human urine samples of different age group (20, 40 and 60) using standard addition method with commercial DA spiked to the solution. The present modified electrode shows good recovery for the determination of DA in human urine samples which is tabulated in Table 2. As expected, the level of DA is found to increase with the increase of age. Hence the present sensor can be conveniently used for the determination DA in human urine samples.

4. CONCLUSIONS

The *in-situ* synthesis of a new ternary polypyrrole-silver-polyvinylpyrrolidone nonocomposite using $AgNO_3$ as an oxidant and polyvinyl pyrrolidone as a stabilizer and surfactant has been demonstrated. The synthesized PPy-Ag-PVP has been investigated for its selective and sensitive sensing of dopamine (DA). The developed PPy-Ag-PVP shows a simple and versatile protocol which provides an effective linearity range, limit of detection and limit of quantification which are found to be 100nM to 900 nM, 0.0126 and 0.042 μM (S/N = 3 & 10) respectively with remarkable sensitivity (7.26 μA mM^{-1} cm^{-2}). The practical application of the present modified electrode has been validated by determining the concentration of DA in human urine samples of different age group. It is envisaged that the proposed sensor material will be beneficial for biological and environmental applications.

REFERENCES

1. Ensafi, A.; Taei, M.; Khayamian, T. A Differential Pulse Voltammetric Method for Simultaneous Determination of Ascorbic acid, Dopamine, and Uric acid using Poly (3- (5-chloro- 2 –hydroxy phenyl azo) -4,5-dihydroxy naphthalene-2,7-disulfonic acid) Film Modified Glassy Carbon Electrode. *J. Electroanal. Chem.* **2009**, *633,* 212-220.

2. Hou, S. R.; Zheng, N.; Feng, H. Y.; Li, X. J.; Yuan, Z. B. Determination of Dopamine in the Presence of Ascorbic Acid using Poly(3,5-dihydroxy benzoic acid) film Modified Electrode. *Anal. Biochem*. **2008**,*179,* 179-184.

3. Jia, N. Q.; Wang, Z. Y.; Yang, G. F.; Shen, H. B.; Zhu, L. Z. Electrochemical Properties of Ordered Mesoporous Carbon and Its Electroanalytical Application for Selective Determination of Dopamine. *Electrochem. Commun*. **2007**, *9,* 233-238.

4. Mo, J. W.; Ogorevc, B. Simultaneous Measurement of Dopamine and Ascorbate at their Physiological Levels using Voltammetric Microprobe based on over Oxidized Poly(1, 2-phenylene diamine)-Coated Carbon Fiber. *Anal. Chem*. **2001**, *73,* 1196-1202.

5. Shang, N. G.; Papakonstantinou, P.; McMullan, M.; Chu, M.; Stamboulis, A.; Potenza, A.; Dhesi, S. S.; Marchetto, H. Catalyst Free Efficient Growth, Orientation and Biosensing Properties of Multilayer Graphene Nanoflake Films with Sharp Edge Planes. *Adv. Funct. Mater.* **2008,** *18,* 3506-3514.

6. Phillips, P. E. M.; Stuber, G. D.; Heien, M.; Wightman, R. M.; Carelli, R. M. Subsecond Dopamine Release Promotes Cocaine Seeking. *Nature* **2003,** *422,* 614-618.

7. Wilson, G. S.; Johnson, M. A. In-Vivo Electrochemistry: What Can We Learn about Living Systems?. *Chem. Rev.* **2008,** *108,* 2462-2481.

8. Smythies, J. The Neurotoxicity of Glutamate, Dopamine, Iron and Reactive Oxygen Species: Functional Interrelationships in Health and Disease: A Review — Discussion. *Neurotoxic. Res.* **1999,** *1,* 27-39.

9. Lee, T.; Cai, L. X.; Lelyveld, V. S.; Hai, A.; Jasanoff, A. Molecular-Level Functional Magnetic Resonance Imaging of Dopaminergic Signaling. *Science* **2014,** *344,* 533-535.

10. VanDersarl, J. J.; Mercanzini, A.; Renaud, P. Integration of 2d and 3d Thin Film Glassy Carbon Electrode Arrays for Electrochemical Dopamine Sensing in Flexible Neuroelectronic Implants. *Adv. Funct. Mater.* **2015,** *25,* 78-84.

11. Zhang, M.; Liao, C.; Yao, Y.; Liu, Z.; Gong, F.; Yan, F. High-Performance Dopamine Sensors Based on Wholegraphene Solution- Gated Transistors. *Adv. Funct. Mater.* **2014,** *24,* 978-985.

12. Li, B.-R.; Hsieh, Y.-J.; Chen, Y.-X.; Chung, Y.-T.; Pan, C.-Y.; Chen, Y.-T. An Ultrasensitive Nanowire-Transistor Biosensor for Detecting Dopamine Release from Living Pc12 Cells Under Hypoxic Stimulation. *J. Am. Chem. Soc.* **2013,** *135,* 16034-16037.

13. Lowa, K.; Hornera, C. B.; Lib, C.; Icoa, G.; Boszeb, W.; Myungb, N. V.; Nam, J. Composition-Dependent Sensing Mechanism of Electrospun Conductive Polymer Composite Nanofibers. *Sens. Actuators, B* **2015,** *207,* 235-242.

14. Xue, C.; Han, Q.; Wang, Y.; Wu, J. H.; Wen, T. T.; Wang, R. Y.; Hong, J. L.; Zhou, X. M.; Jiang, H. J. Amperometric Detection of Dopamine in Human Serum by Electrochemical Sensor Based on Gold Nanoparticles Doped Molecularly Imprinted Polymers. *Biosens. Bioelectron.* **2013,** *49,* 199-203.

15. Ballesteros, C. A. S.; Cancino, J.; Marangoni, V. S.; Zucolotto, V. Nanostructured Fe_3O_4 Satellite Gold Nanoparticles to Improve Biomolecular Detection. *Sens. Actuators, B* **2014,** *198,* 377-383.

16. Huang, Y.; Miao, Y.-E.; Ji, S.; Tjiu, W. W.; Liu, T. Electrospun Carbon Nanofibers Decorated with Ag−Pt Bimetallic Nanoparticles for Selective Detection of Dopamine. *ACS Appl. Mater. Interfaces* **2014,** *6,* 12449-12456.

17. Gao, F.; Cai, X. L.; Wang, X.; Gao, C.; Liu, S. L.; Gao, F.; Wang, Q. X. Highly Sensitive and Selective Detection of Dopamine in the Presence of Ascorbic Acid at Graphene Oxide Modified Electrode. *Sens. Actuators, B* **2013,** *186,* 380-387.

18. Dong, X.; Wang, X.; Wang, L.; song, H.; Zang, H.; Huang, W.; Chen, P. 3D Graphene Foam as a Monolithic and Macroporous Carbon Electrode for Electrochemical Sensing. *ACS Appl. Mater. Interfaces* **2012,** *4,* 3129-3133.

19. Zhao, J.; Zhang, W.; Sherrell, P.; Razal, J. M.; Huang, X.-F.; Minett, A. I.; Chen, J. Carbon Nanotube Nanoweb-Bioelectrode for Highly Selective Dopamine Sensing. *ACS Appl. Mater. Interfaces* **2012,** *4,* 44-48.

20. Shakkthivel, P.; Chen, S. M. Simultaneous Determination of Ascorbic Acid and Dopamine in the Presence of Uric Acid on Ruthenium Oxide Modified Electrode. *Biosens. Bioelectr.* **2007,** *22,* 1680-1687.

21. Mahshid, S.; Li, C. C.; Mahshid, S. S.; Askari, M.; Dolati, A.; Yang, L. X.; Luo, S. L.; Cai, Q. Y. Sensitive Determination of Dopamine in the Presence of Uric Acid and Ascorbic Acid Using TiO_2 Nanotubes Modified with Pd, Pt and Au Nanoparticles. *Analyst* **2011,** *136,* 2322-2329.

22. Kohlman, R. S.; Epstein, A. J. *Handbook of Conducting Polymers*, 2nd ed, Marcel Dekker, New York, **1998,** p. 85.

23. Acar, H.; Karakısla, M.; Sacak, M. Preparation and Characterization of Conductive Polypyrrole/kaolinite Composites. *Mat. Sci. Semi. Proces.* **2013,** *16,* 845-850.

24. Lee, Y. H.; Lee, J. Y.; Lee, D. S. A Novel Conducting Soluble Polypyrrole Composite with a Polymeric Co-dopant. *Synth Met*. **2000**, *114,* 347-353.

25. Palanisamy, S.; Thirumalraj, B.; Chen, S-M.; Ajmal Ali, M.; Muthupandi, K.; Emmanuel, R.; Prakash, P.; Al-Hemaid, F. M. A. Fabrication of Silver Nanoparticles Decorated on Activated

Screen Printed Carbon Electrode and Its Application for Ultrasensitive Detection of Dopamine. *Electroanalysis* **2015**, *27,* 1998-2006.

26. Ghadim, M. F.; Imani, A.; Farzi, G. Synthesis of PPy–Silver Nanocomposites via In Situ Oxidative Polymerization. J. Nanostruct. Chem. **2014,** *4,* 101.
27. Feng, X.; Huang, H.; Ye, Q.; Zhu, J-J.; Hou, W. Ag/Polypyrrole Core-Shell Nanostructures: Interface Polymerization, Characterization, and Modification by Gold Nanoparticles. *J. Phys. Chem. C* **2007,** *111,* 8463-8468.
28. Yan, G.; Peng, J.; Li, S.; Lifeng, L.; Xiaoqin ,Y.; Zhenping, Z.; Dongfang, L.; Jianxiong, W; Huajun, Y.; Zengxing, Z.; Xiaowei, Z.; Xinyuan, D.; Weiya, Zhou, Gang W.; Sishen, X. Growth Mechanism of Silver Nnanowires Synthesized by Polyvinylpyrrolidone-assisted Polyol Reduction, *J. Phys. D: Appl. Phys.* **2005,** *38,* 1061–1067.
29. Jin, L.; Huiqing, F.; Jin, C.; Laijun, L. Synthesis and Characterization of Poly (vinyl pyrrolidone) - Capped Bismuth Nanospheres, *Colloids and Surfaces A,* **2009,** *340,* 66–69
30. Na, S.; Huiqing, F.; Hailin, T. PVP Assisted In Situ Synthesis of Functionalized Graphene/ZnO (FGZnO) Nanohybrids with Enhanced Gas-Sensing Property, *J. Mater. Sci.* **2015,** *50,* 2229–2238.
31. Yang, C.; Liu, P. Water-Dispersed Polypyrrole Nanoparticles via Chemical Oxidative Polymerization in the Presence of a Functional Polyanion. *React. & Funct. Polym*. **2010**, *70,* 726-731.
32. Woo, H. Y.; Jung, W. G.; Ihm, D. W.; Kim, J. Y. Synthesis and Dispersion of Polypyrrole Nanoparticles in Polyvinylpyrrolidone Emulsion. *Synth. Met*. **2010**, *160,* 588-591.
33. Balakumar, V.; Prakash, P. Silver-Nanospheres as a Green Catalyst for the Decontamination of Hazardous Pollutants. *RSC Adv*. **2015**, *5,* 105917-105924.

34. Stankovich, S.; Dikin, D. A.; Piner, R. D.; Kohlhaas, K. A.; Kleinhammes, A.; Jia, Y.; Wu, Y.; Nguyen, S. T.; Ruoff, R. S. Synthesis of graphene-based Nanosheets via Chemical Reduction of Exfoliated Graphite Oxide. *Carbon* **2007**, *45,* 1558-1565.

35. Qian, Y-F.; Yin, J.; Feng, S.; Liu, S-H.; Zhu, Z-K. Preparation and Characterization of Polyvinylpyrrolidone Films Containing Silver Sulfide Nanoparticles. *J. Mater. Chem*. **2001**, *11,* 2504-2506.

36. Kuilla, T.; Bhadra, S.; Yao, D.; Kim, N. H.; Bose, S.; Lee, J. H. Recent Advances in Graphene based Polymer Composites. *Prog. Polym. Sci*. **2010**, *35,* 1350-1375.

37. Liu, Y. C.; Lee, H. T.; Yang, S. J. Strategy for the Syntheses of Isolated Fine Silver Nanoparticles and Polypyrrole/Silver Nanohybrids on Gold Substrates. *Electrochim. Acta*. **2006**, *51,* 3441-3445.

38. Mikat, J.; Orgzall, I.; Hochheimer, H. D. Optical absorption and vibrational spec-troscopy of conducting polypyrrole under presuure. *Synth. Met.* **2001,** *116,* 167-170.

39. Han, Y.; Lu, Y. Preparation and Characterization of Graphite Oxide/Polypyrrole Composites. Carbon. **2007**, *45,* 2394-2399.

40. Yan, F.; Xue, G.; Zhou, M. J. Preparation of Electrically Conducting Polypyrrole in Oil/Water Microemulsion. *Appl. Polym. Sci*. **2000**, *77,* 135-140.

41. Omastova, M.; Trchova, M.; Pionteck, J.; Prokes, J.; Stejskal, J. Effect of Polymerization Conditions on the Properties of Polypyrrole Prepared in the Presence of Sodium bis(2-ethylhexyl) sulfosuccinate. *Synth. Met*. **2004**,*143,* 153-161.

42. Raina, S.; Kang, W. P.; Davidson, J. L. Nitrogen Incorporated Nanodiamond Film with 'Ridge' Surface Morphology for Detection of Bio-analyte. *Diamond Relat. Mater*. **2009**, *18,* 574-577.

43. Li, P.; Li, J.; Wu, C.; Wu, Q.; Li, J. Synergistic Antibacterial Effects of β-Lactam Antibiotic Combined with Silver Nanoparticles. *Nanotechnology*. **2005**, *16,* 1912-1917.

44. Zhang, W.; Yuan, R.; Chai, Y-Q.; Zhang, Y.; Chen, S-H. A Simple Strategy based on Lanthanum–Multiwalled Carbon Nanotube Nanohybrids for Simultaneous Determination of Ascorbic acid, Dopamine, Uric Acid and Nitrite. *Sens. Actuators B* **2012,** *166–167,* 601-607.

45. Thiagarajan, S.; Yang, R. F.; Chen, S-M.; Palladium Nanoparticles Modified Electrode for the Selective Detection of Catecholamine Neurotransmitters in Presence of Ascorbic Acid. *Bioelectrochemistry* **2009,** *75,* 63-169.

46. Prabakar, S. J. R.; Narayanan, S. S. Catalytic Oxidation of Dopamine at a Nickel Hexacyanoferrate Surface Modified Graphite Wax Composite Electrode Coated with Nafion. *Electroanalysis* **2009,** *21,* 1481–1489.

47. Ge, P.-Y.; Du, Y.; Xu, J.-J.; Chen, H.-Y. Selective Detection of Dopamine Based on the Unique Property of Gold Nanofilm. *J. Electroanal. Chem*. **2009**, *633,* 182-186.

48. Kim, Y-R.; Bong, S.; Kang, Y-J.; Yang, Y.; Mahajan, R. K.; Kim, J. S.; Kim, H. Electrochemical Detection of Dopamine in the Presence of Ascorbic Acid using Grapheme Modified Electrodes. *Biosens. Bioelectron.* 2**010,** *25,* 2366–2369

49. Chen, S.; Yang, W.; Chen, X.; Highly Sensitive and Selective Determination of Dopamine Based on Graphite Nanosheet-Nafion Composite Film Modified Electrode. *Electroanalysis* **2010,** *22,* 908–911.

50. Sheng, Z-H.; Zheng, X-Q.; Xu, J-Y.; Bao, W-J.; Wang, F-B.; Xia, X-H. Electrochemical Sensor Based on Nitrogen Doped Graphene: Simultaneous Determination of Ascorbic Acid, Dopamine And Uric Acid. *Biosens. Bioelectron.* **2012,** *34,* 125–131.

51. Yue, Y.; Hu, G.; Zheng, M.; Guo, Y.; Cao, J.; Shao, S. A Mesoporous Carbon Nanofiber-Modified Pyrolytic Graphite Electrode used for the Simultaneous Determination of Dopamine, Uric Acid, and Ascorbic Acid. *Carbon* **2012,** *50,* 107–114.

52. Dong, X.; Wang, X.; Wang, L.; song, H.; Zang, H.; Huang, W.; Chen, P. 3D Graphene Foam as a Monolithic and Macroporous Carbon Electrode for Electrochemical Sensing. *ACS Appl. Mater. Interfaces* **2012,** *4,* 3129-3133.

53. Hsu, S-M.; Chen, Y. L.; Lee, C. Y.; Chiu, H. T. Gold Nanostructures on Flexible Substrates as Electrochemical Dopamine Sensors. *ACS Appl. Mater. Interfaces* **2012,** *4,* 5570-5575.

54. Kan, X.; Zhou, H.; Li, C.; Zhu, A.; Xing, Z.; Zhao, Z. Imprinted Electrochemical Sensor for Dopamine Recognition and Determination Based on a Carbon Nanotube/Polypyrrole Film. *Electrochim. Acta* **2012**, *63,* 69-75.

55. Wang, X.; Wu, M.; Tang, W.; Zhu, Y.; Wang, L.; Wang, Q.; He, P.; Fang, Y. Simultaneous Electrochemical Determination of Ascorbic acid, Dopamine and Uric Acid using a Palladium Nanoparticle/Graphene/Chitosan Modified Electrode. *J. Electroanal. Chem.* **2013,** *695,* 10-16.

56. Reddaiah, K.; Reddy, T M.; Mallikarjun, K.; Narasimha, G. Electrochemical Detection of Dopamine at Poly(solochrome cyanine)/Pd Nanoparticles Doped Modified Carbon Paste Electrode and Simultaneous Resolution in the Presence of Ascorbic Acid and Uric Acid: A Voltammetric Method. *Anal. Methods* **2013,** *5,* 5627-5636.

57. Ling, Y-Y.; Huang, Q-A.; Zhu, M-S.; Feng, D-X.; Li, X-Z.; Wei, Y. A Facile One-step Electrochemical Fabrication of Reduced Graphene Oxide–Mutilwall Carbon Nanotubes–Phospotungstic Acid composite for Dopamine Sensing. *J. Electroanal. Chem.* **2013,** *693*, 9–15.

58. Ku, S.; Palanisamy, S.; Chen, S-M. Highly Selective Dopamine Electrochemical Sensor Based on Electrochemically Pretreated Graphite and Nafion Composite Modified Screen Printed Carbon Electrode. *J. Coll. Inter. Sci.* **2013,** *411,*182–186.

59. Jiang, J.; Du, X. Sensitive Electrochemical Sensors for Simultaneous Determination of Ascorbic Acid, Dopamine, and Uric Acid based on Au@Pd-reduced Graphene Oxide Nanohybrids. *Nanoscale* **2014,** *6,* 11303-11309.

60. Palanisamy, S.; Thirumalraj, B.; Chen, S-M. Palladium Nanoparticles Decorated on Activated Fullerene Modified Screen Printed Carbon Electrode for Enhanced Electrochemical Sensing of Dopamine. *J. Coll. Inter. Sci.* **2015,** *448,* 251-256.

61. Wang, S.; Zhang, W.; Zhong, X.; Chai, Y.; Yuan, R. Simultaneous Determination of Dopamine, Ascorbic Acid and Uric Acid using a Multi-Walled Carbon Nanotube and Reduced Graphene Oxide Hybrid Functionalized by PAMAM and Au Nanoparticles. *Anal. Methods* **2015,** *7,* 1471–1477.

62. Zhong, M.; Teng, Y.; Pang, S.; Yan, L.; Kan, X. Pyrrole–Phenylboronic Acid: A Novel Monomer for Dopamine Recognition and Detection Based on Imprinted Electrochemical Sensor. *Biosens. Bioelectron.* **2015,** *64,* 212-218.

63. Kannan, P. K.; Moshkalev, S. A.; Rout, C. S. Highly Sensitive and Selective Electrochemical Dopamine Sensing Properties of Multilayer Graphene Nanobelts. *Nanotechnology* **2016,** *27,* 075504.

64. Mahmoudian, M. R.; Basirun, W. J.; Alias, Y. B. A Sensitive Dopamine Biosensor Based on Polypyrrole Coated Palladium Silver Nanospherical Composites. *Ind. Eng. Chem. Res.* **2016**, *55,* 6943–6951.

Scheme, Figure and Table Captions

Scheme 1 The schematic representation of in-situ synthesis of PPy-Ag-PVP nanohybrid

Figure. 1(A) UV-vis absorbance spectra of PPy-Ag-PVP (1) (black line), PPy-Ag-PVP (2) (red line) and PPy-Ag-PVP (3) (blue line), (B) FT-IR spectra of (a) PPy-Ag-PVP (1), (b) PPy-Ag-PVP (2) and (c) PPy-Ag-PVP (3), (C) XRD patterns of (a) PPy-Ag-PVP (1), (b) PPy-Ag-PVP (2) and (c) PPy-Ag-PVP (3) and (D) Raman spectra of (a) PPy-Ag-PVP (1), (b) PPy-Ag-PVP (2) and (c) PPy-Ag-PVP (3) nanohybrid

Figure. 2 SEM images of (a) PPy-Ag-PVP (1), (b) PPy-Ag-PVP (2) and (c) PPy-Ag-PVP (3) nanohybrid

Figure. 3 HR-TEM images of (a) PPy-Ag-PVP (1), (b) PPy-Ag-PVP (2), (c) PPy-Ag-PVP (3) nanohybrid, (d & e) HR-EM images of PPy-Ag-PVP (2) with different magnifications and (f) SAED pattern of PPy-Ag-PVP (2)

Figure. 4 TGA analysis of PPy-Ag-PVP (2) nanohybrid

Figure. 5 CV response of (A (curve a)) PPy-Ag-PVP (2) modified GCE and (curve b) PPy-Ag-PVP (2) modified GCE at a scan rate of 50 mV/s in 0.1 M PBS (pH = 7.2) containing 50 μM DA, (B) CV response of the PPy-Ag-PVP (2) modified GCE in 0.1 M PBS (pH=7.2) with different concentrations of DA: (a) 10, (b) 20, (c) 30, (d) 40, (e) 50, (f) 60, (g) 70, (h) 80, (i) 90 and (j) 100 μM and (C) The calibration plot for the linear dependence of DA vs I_{pc}

Figure. 6 Mechanism for the electrochemical sensing of DA using PPy-Ag-PVP (2)

Figure. 7 CVs of (A) Py-Ag-PVP (2) modified GCE in 0.1 M PBS (pH=7.2) containing 50 μM DA with different scan rates, (a) 50, (b) 60, (c) 70, (d) 80, (e) 90, (f) 100, (g) 110, (h) 120, (i) 130 and (j)

140 mV s^{-1}, (B) The calibration plot for the linear dependence of oxidation and reduction peak current vs scan rate, (C) Effect of pH on the peak current and (D) Effect of pH on peak potential for the oxidation of 50 μM DA in 0.1 M PBS (pH=7.2)

Figure. 8 (A) DPV response of PPy-Ag-PVP (2) modified GCE in 0.1 M PBS (pH=7.2) with different concentrations of DA: (a) 0.5, (b) 2.5, (c) 5.0, (d) 7.5, (e) 10.0, (f) 12.5, (g) 15.0, (h) 17.5, (i) 20.0 and (j) 22.5 μM, (B) The plot of concentration of DA vs I_{pc}. (C) Amperometric i–t curve for the determination of DA at Py-Ag-PVP (2) modified GCE in 0.2 M PB solution (pH 7.2) and (D) The calibration plot for the linear dependence of peak current vs concentrations of DA

Figure. 9 Amperometric response of the interference test for Py-Ag-PVP (2) modified GCE to successive additions of 200 nM DA and 20 fold excess of AA, UA, FA, glucose, sucrose, fructose and 200 nM DA with stirring in 0.1 M PBS (pH 7.2) at a potential of 0.132 V

Figure. 10 Electrochemical impedance spectra (a) of the PPy-Ag-PVP (2) modified electrode (black line) and after 15-day storage in 1M (pH=7.2) PBS (red line) and FT-IR spectra (b) of the PPy-Ag-PVP (2) (black line) and after 15-day storage in 1M (pH=7.2) PBS (red line)

Table 1 Comparison of DA sensors based on different electrode materials

Table 2 Determination of DA in urine samples of different age group

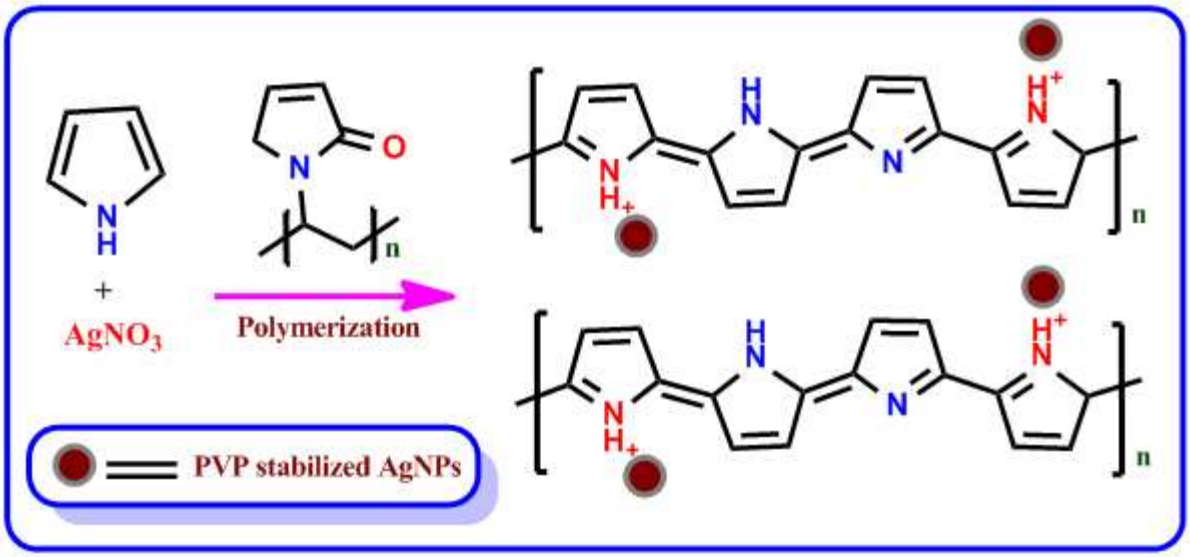

Scheme 1

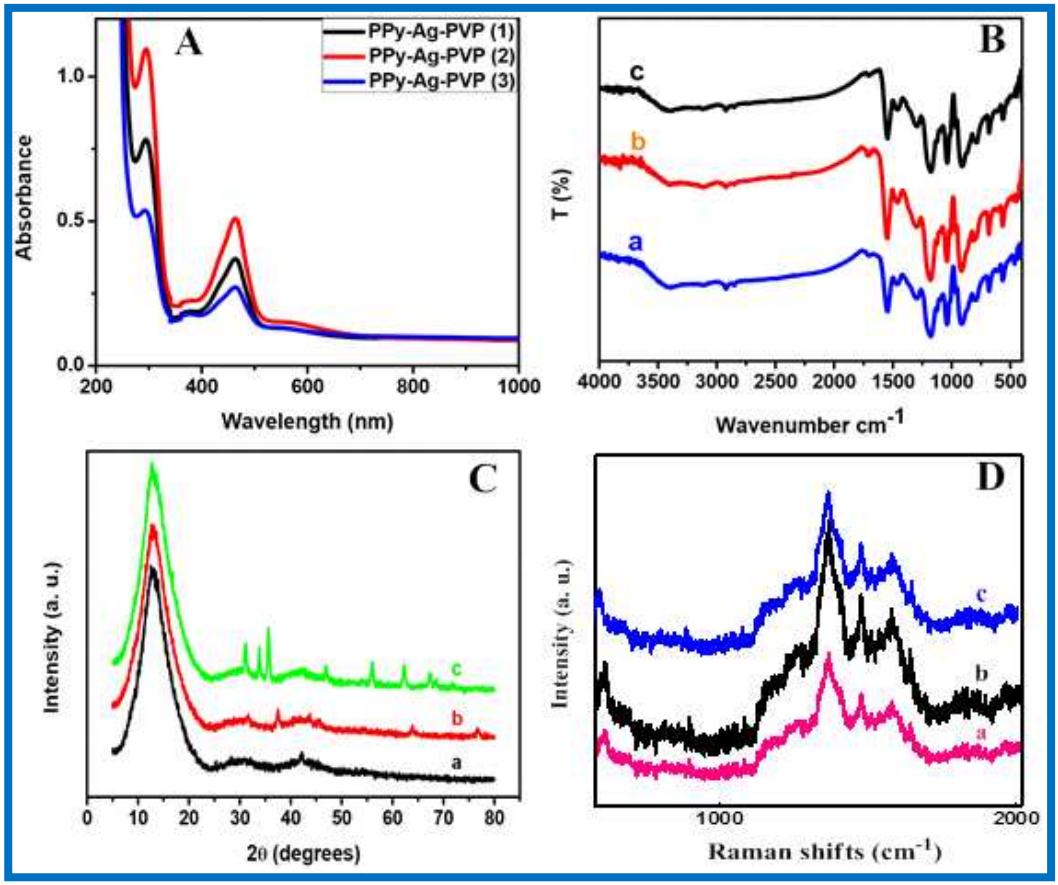
A
PPy-Ag-PVP (1)
PPy-Ag-PVP (2)
PPy-Ag-PVP (3)
Absorbance
Wavelength (nm)
B
c
b
a
T (%)
Wavenumber cm-1
C
Intensity (a. u.)
2θ (degrees)
D
Intensity (a. u.)
Raman shifts (cm-1)

Figure. 1

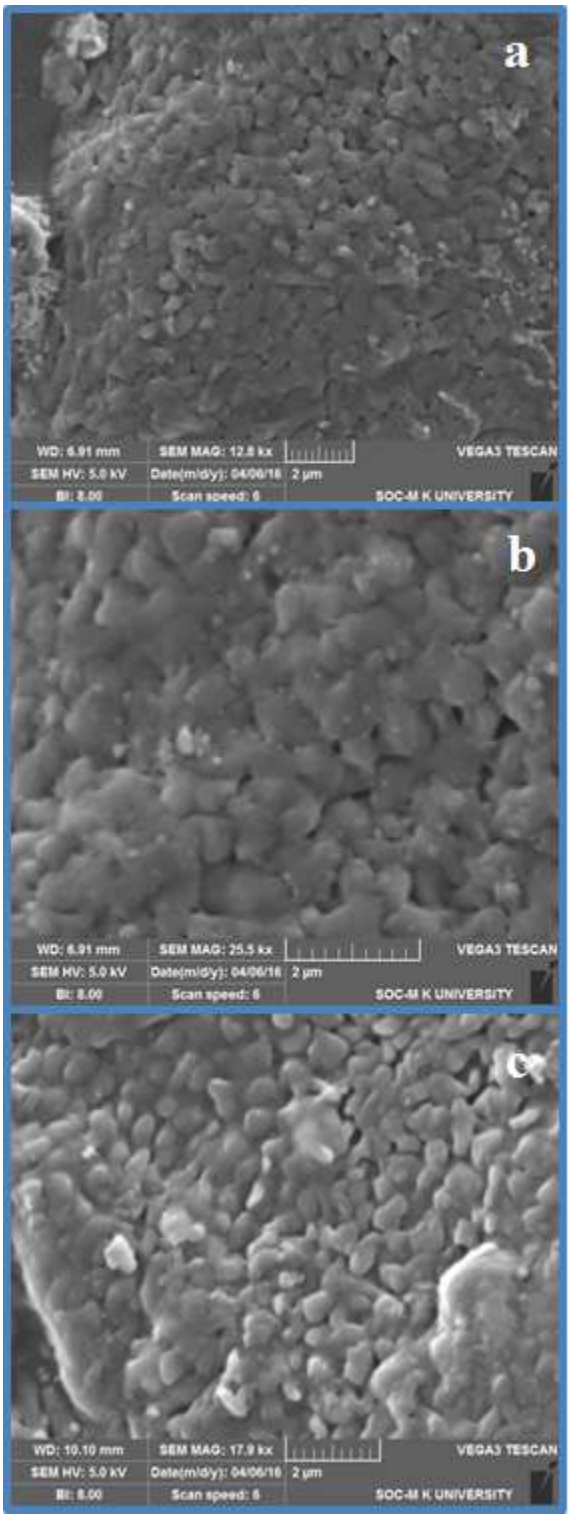
a
WD: 6.91 mm
SEM MAG: 12.8 kx
VEGA3 TESCAN
SEM HV: 5.0 kV
Date(m/d/y): 04/06/16
2 µm
BI: 8.00
Scan speed: 6
SOC-M K UNIVERSITY
b
WD: 6.91 mm
SEM MAG: 25.5 kx
VEGA3 TESCAN
SEM HV: 5.0 kV
Date(m/d/y): 04/06/16
2 µm
BI: 8.00
Scan speed: 6
SOC-M K UNIVERSITY
c
WD: 10.10 mm
SEM MAG: 17.9 kx
VEGA3 TESCAN
SEM HV: 5.0 kV
Date(m/d/y): 04/06/16
2 µm
BI: 8.00
Scan speed: 6
SOC-M K UNIVERSITY

Figure. 2

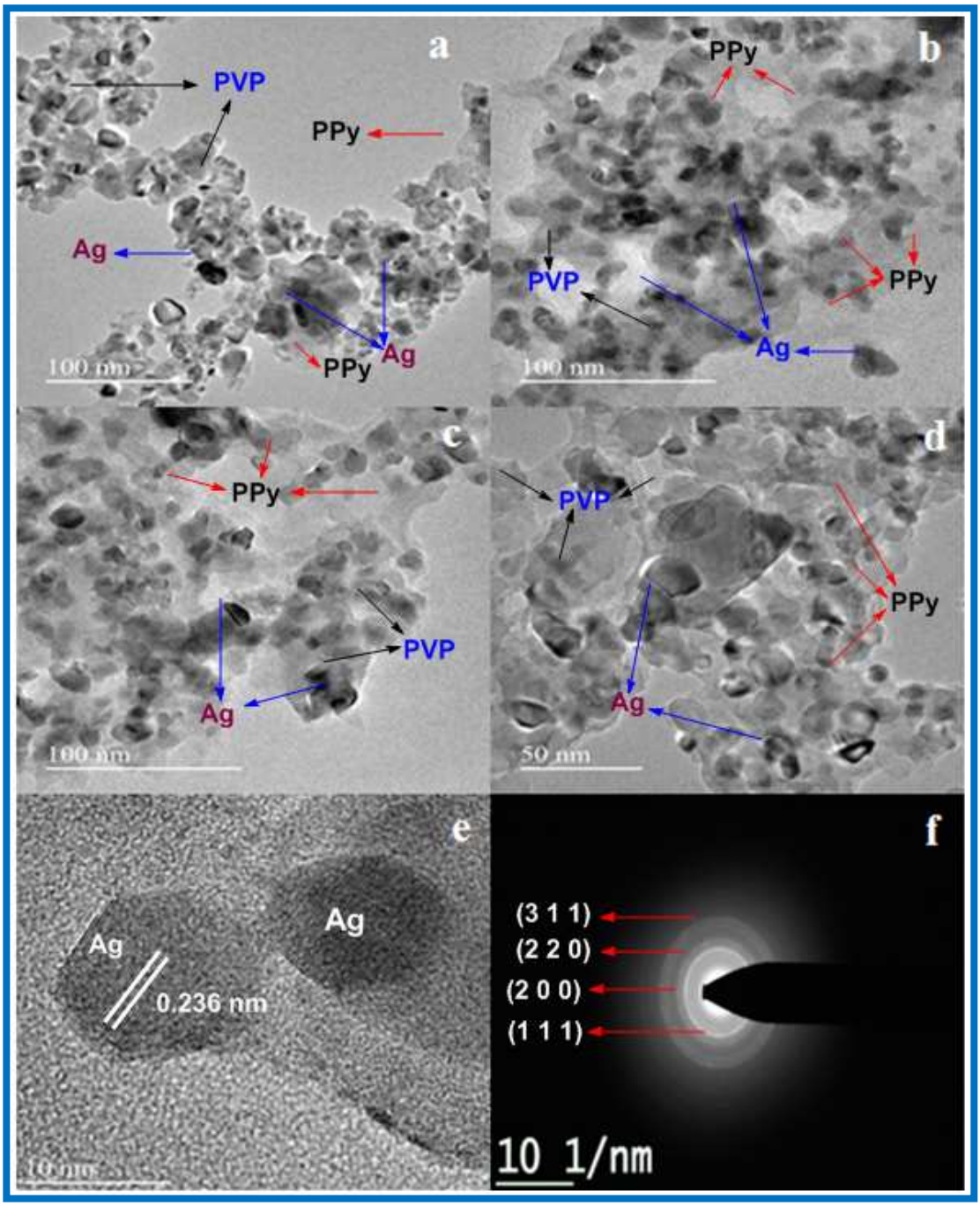
a
PVP
PPy
Ag
Ag
PPy
100 nm
b
PPy
PVP
PPy
Ag
100 nm
c
PPy
PVP
Ag
100 nm
d
PVP
PPy
Ag
50 nm
e
Ag
Ag
0.236 nm
10 nm
f
(3 1 1)
(2 2 0)
(2 0 0)
(1 1 1)
10 1/nm

Figure. 3

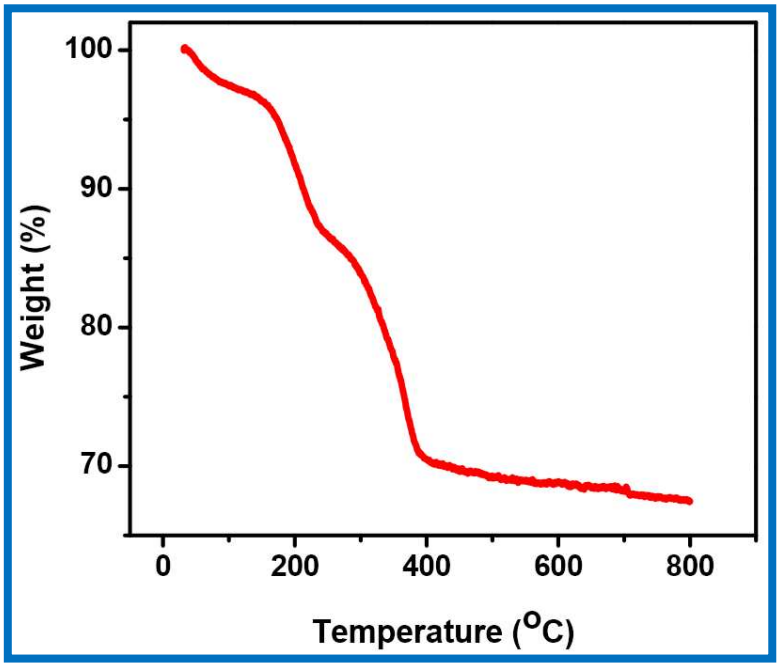

Figure. 4

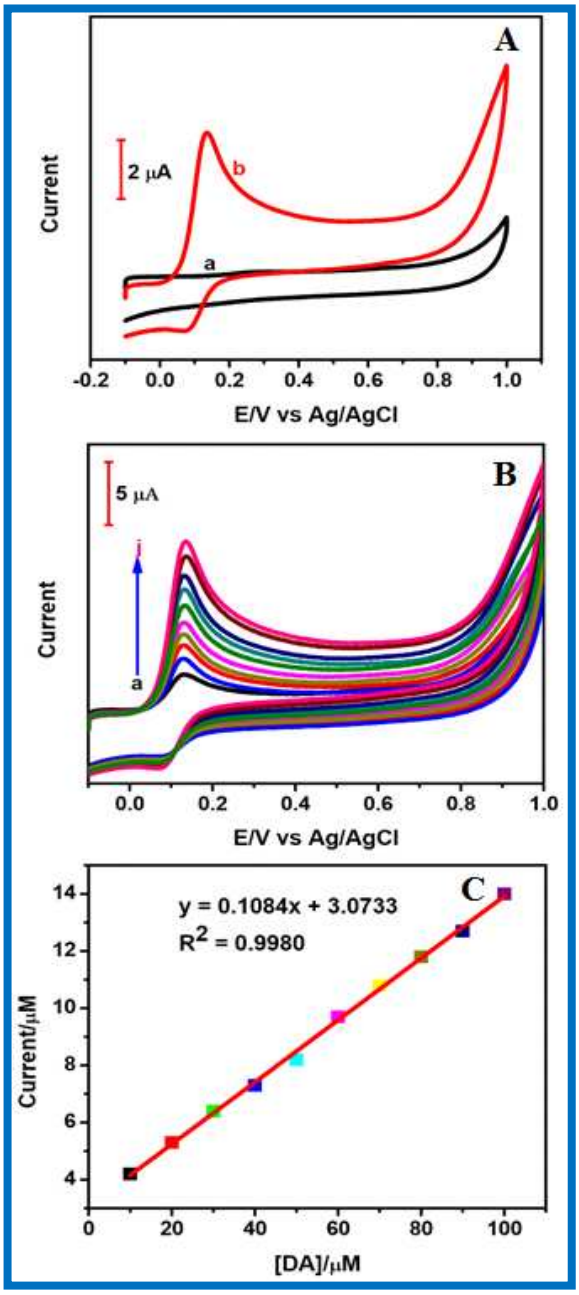
A
2 μA
b
a
Current
-0.2
0.0
0.2
0.4
0.6
0.8
1.0
E/V vs Ag/AgCl
B
5 μA
j
a
Current
0.0
0.2
0.4
0.6
0.8
1.0
E/V vs Ag/AgCl
C
y = 0.1084x + 3.0733
R2 = 0.9980
Current/μM
4
6
8
10
12
14
0
20
40
60
80
100
[DA]/μM

Figure. 5

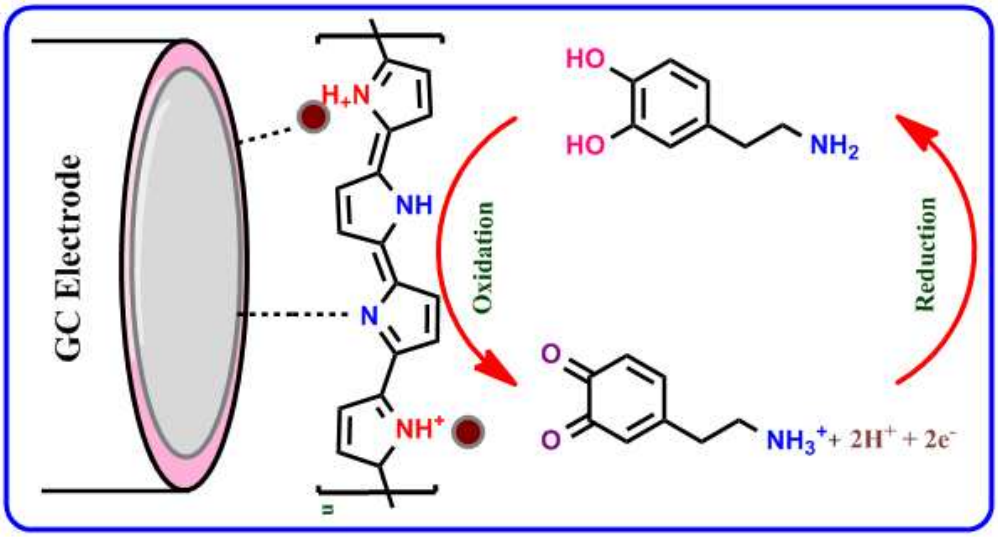
GC Electrode
H₂N
NH
N
NH⁺
Oxidation
Reduction
HO
HO
NH₂
O
O
NH₃⁺ + 2H⁺ + 2e⁻

Figure. 6

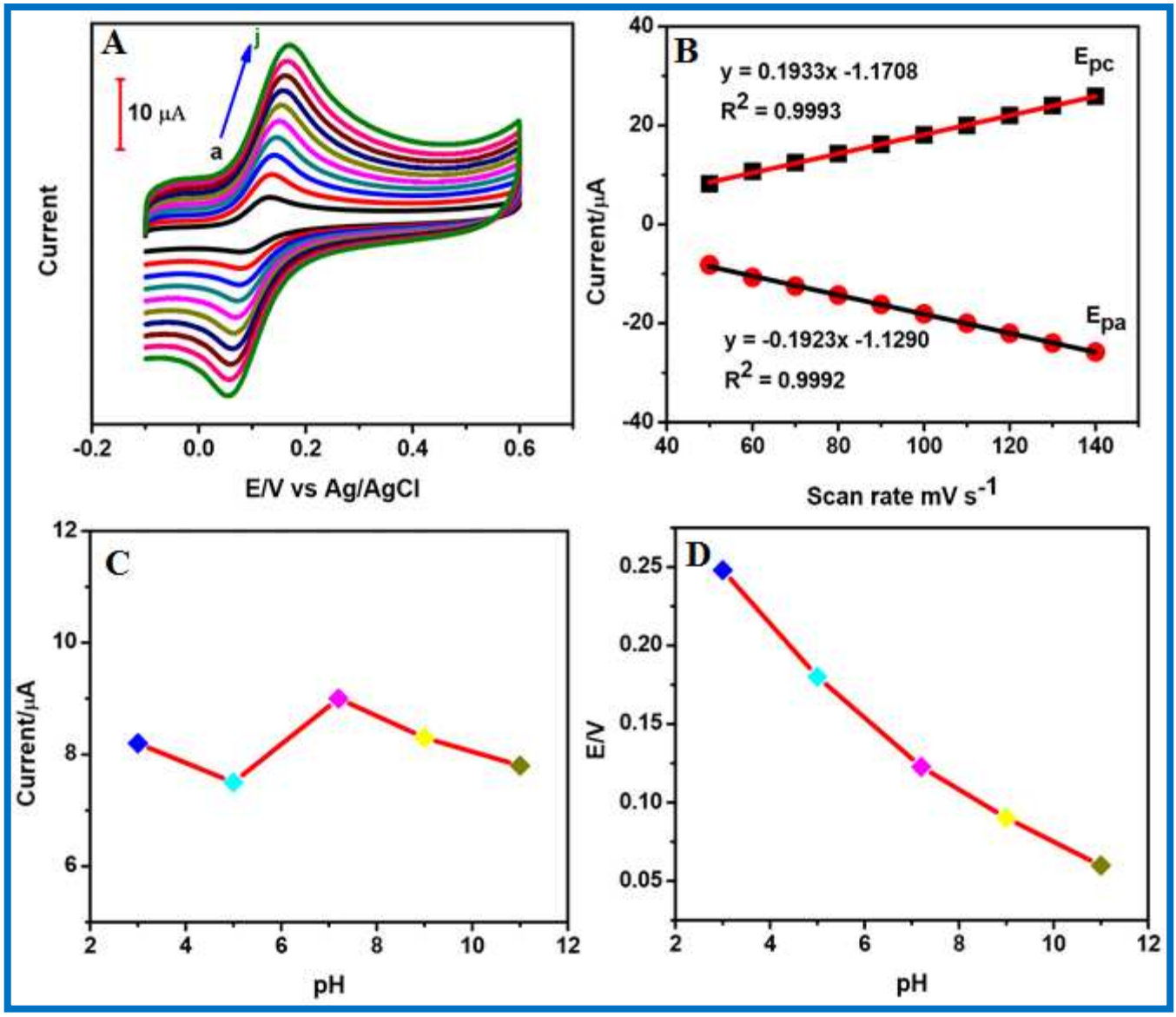
A
10 μA
a
j
Current
E/V vs Ag/AgCl
B
y = 0.1933x -1.1708
R2 = 0.9993
Epc
y = -0.1923x -1.1290
R2 = 0.9992
Epa
Current/μA
Scan rate mV s-1
C
Current/μA
pH
D
E/V
pH

Figure. 7

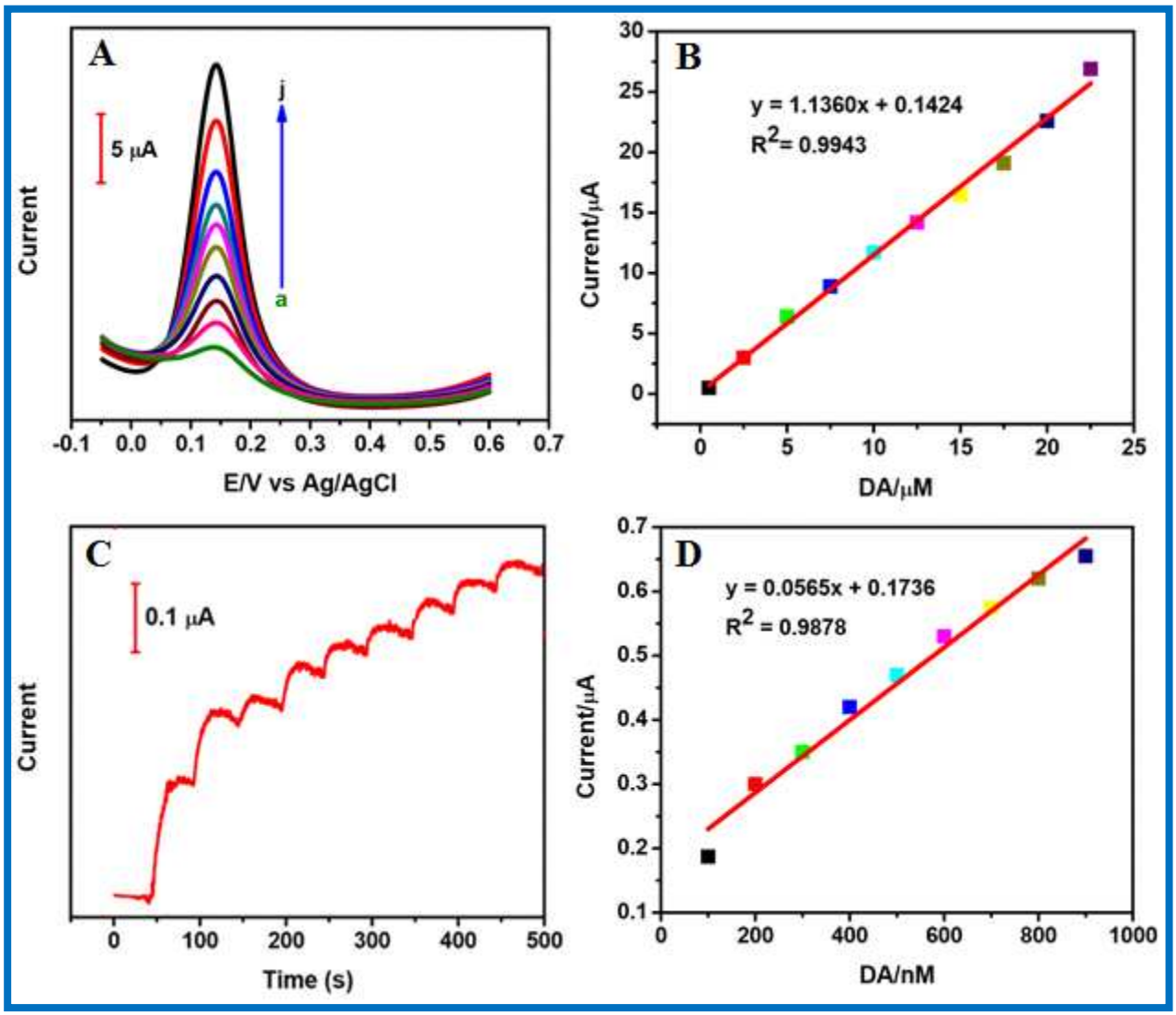
A
5 μA
j
a
Current
-0.1 0.0 0.1 0.2 0.3 0.4 0.5 0.6 0.7
E/V vs Ag/AgCl
B
y = 1.1360x + 0.1424
R2= 0.9943
Current/μA
0 5 10 15 20 25 30
0 5 10 15 20 25
DA/μM
C
0.1 μA
Current
0 100 200 300 400 500
Time (s)
D
y = 0.0565x + 0.1736
R2 = 0.9878
Current/μA
0.1 0.2 0.3 0.4 0.5 0.6 0.7
0 200 400 600 800 1000
DA/nM

Figure. 8

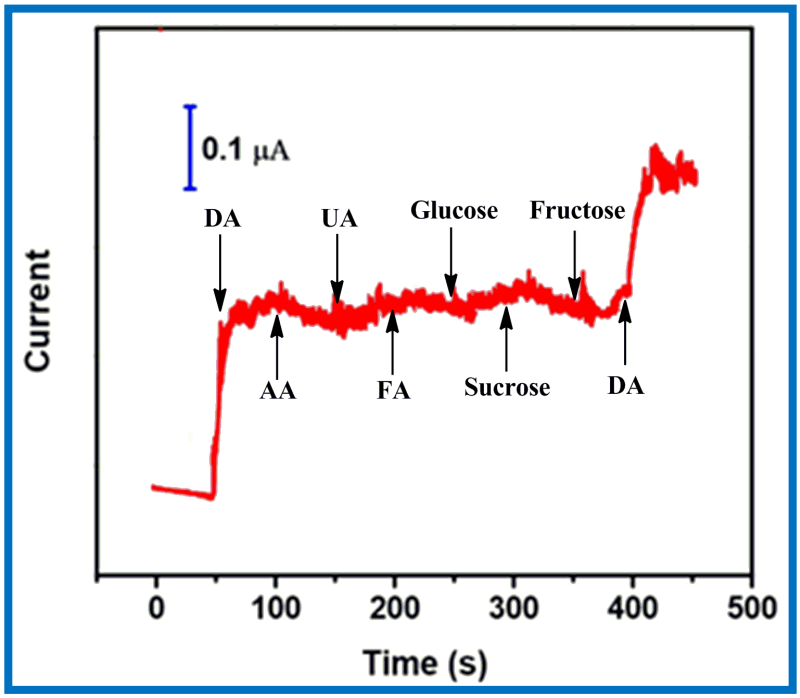
0.1 μA
DA
UA
Glucose
Fructose
AA
FA
Sucrose
DA
Current
0
100
200
300
400
500
Time (s)

Figure. 9

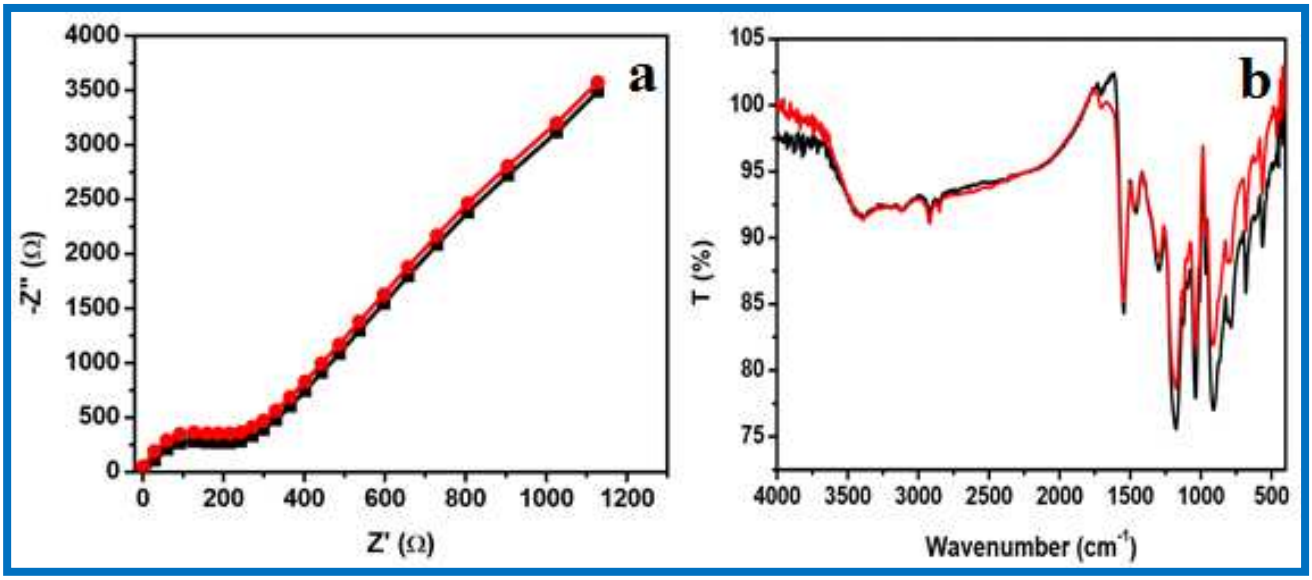
a
-Z'' (Ω)
Z' (Ω)
0
500
1000
1500
2000
2500
3000
3500
4000
0
200
400
600
800
1000
1200
b
T (%)
Wavenumber (cm-1)
75
80
85
90
95
100
105
4000
3500
3000
2500
2000
1500
1000
500

Figure. 10

Table 1

Modified Electrode	Method of Detection	LR (μM)	LOD (μM)	Sensitivity (μA μM^{-1} cm^{-2})	References
PdNPs/GCE	DPV	8-88	-	-	45
NiHCF/graphite wax/nafion	CV	1.5-1200	0.49	0.2053	46
Gold nanofilm	DPV	1.5-27.5	1.50	-	47
Graphene	CV	4-100	2.64	-	48
GNS-Nafion/GC	DPV	0.5-10	0.02	3.695	49
NG	DPV	0.5-170	0.25	-	50
MCNF/PGE	DPV	0.05-30	0.02	-	51
3D graphene	Amp	Upto ~0.25	0.025	619.6	52
Au electrode	Amp	0.22-600	0.026	0.178	53
Molecularly imprinted polymer/MWCN/GCE	DPV	0.625-100	0.06	-	54
PdNPs/GR/CHI/GCE	DPV	0.5–15	0.10	-	55
polySCCy/PdNPs/CPE	CV	-	1.87	-	56
RGO–MWNTs–PTA	DPV	0.5-20	1.14	-	57
Electrochemically pretreated graphite/nafion	LSV	0.5-10	0.023	2.47	58
Au@Pd-RGO/GCE	DPV	0.01–100	0.024	6.08	59
AC60-PdNPs/GCE	DPV	0.35-135.35	0.056	4.23	60
RGO–PAMAM–MWCNT–AuNP	DPV	10-320	3.30	-	61
Molecular imprinting polymer/GCE	DPV	0.05-10	0.033	-	62
ASPCE/AgNPs/SPCE	DPV	0.05–45.35	0.017	7.85	25
GNB	DPV	0.2-200	0.58	0.95	63
PdAg NSPs-PPy	DPV	0.001-200	0.0258	1.574	64
PPy-Ag-PVP (2)	**Amp**	**0.01-0.09**	**0.0126**	**7.256**	**Present work**

Table 2

Urine samples (age group)	Added (μM)	Found (μM)	Recovery (%)
20	0.5	0.506 ± 0.02	101.4 ± 0.04
40	0.5	0.512 ± 0.01	102.4 ± 0.02
60	0.5	0.517 ± 0.02	103.4 ± 0.04

TOC Graphic

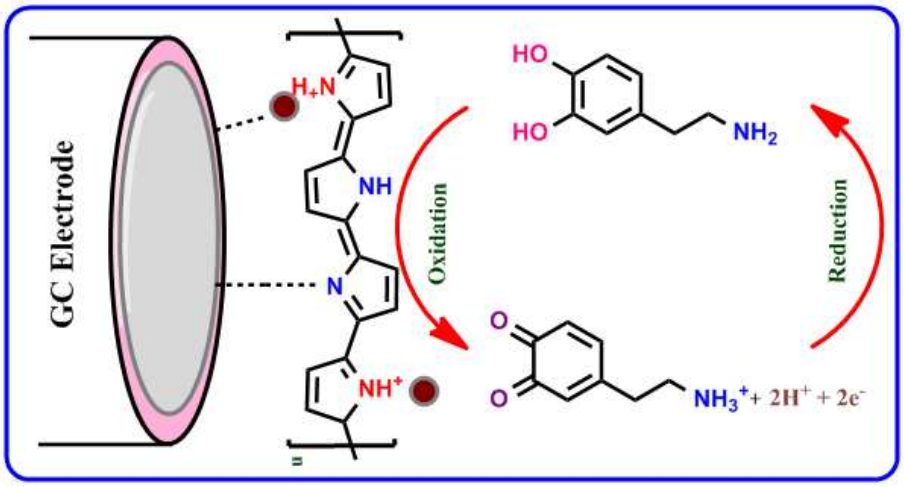
GC Electrode
H2N
NH
N
NH+
Oxidation
Reduction
HO
HO
NH2
O
O
NH3+ + 2H+ + 2e-